PHYSICAL REVIEW A VOLUME 13, NUMBER 1 JANUARY 1976

Electron impact excitation of the $3S$, $3P$, and $3D$ states of H

A. H. Mahan,* A. Gallagher,† and S. J. Smith†

Joint Institute for Laboratory Astrophysics, National Bureau of Standards and University of Colorado, Boulder, Colorado 80302

(Received 2 September 1975)

The relative excitation function for electron-impact excitation of H to yield Balmer α has been measured from threshold to 500-eV collision energy in a crossed-beam apparatus. The relative contributions of the $3S$, $3P$, and $3D$ states to this excitation function have been measured by modulating the electron beam and discriminating on the basis of their different lifetimes for radiative decay after excitation. The resulting set of relative $3S$, $3P$, and $3D$ cross sections has been normalized by equating the total measured Balmer-α cross section at 500 eV to the Born approximation. The normalized cross sections are then compared to available theories at lower energies. In contrast to virtually all known excitation cross sections of neutral atoms, which fall below the Born theory at low energies, the H ($1S \rightarrow 3D$) cross section exceeds the Born theory, apparently owing to coupling between the $3D$ and $2P$ states.

I. INTRODUCTION

This paper reports measurements in a crossed-beam experiment of the relative excitation function for electron-impact excitation of Balmer-α (Hα) emission from atomic hydrogen. In addition, the ratios of the individual contributions to the Hα excitation function by the $3S$, $3P$, and $3D$ states have been measured. The measured relative Hα excitation function, corrected for expected minor polarization and cascading, has been normalized to the Born approximation at 500 eV to yield the Hα direct excitation cross section. The measured ratios of $3S$, $3P$, $3D$ excitation functions have been similarly corrected for minor cascading and polarization to yield these excitation cross sections. The ratios of $3S$, $3P$, and $3D$ cross sections agree with the Born theory at 500 eV, giving support to the reliability of the experimental technique and the normalization at that energy. The cascade corrections, which are typically 5–10%, have been made using $n > 3$ excitation cross sections estimated from ratios of Born cross sections. Polarization corrections to the excitation functions measured perpendicular to the electron beam have been made using the $3P$- and $3D$-state polarizations predicted by the Born approximation. These corrections are a maximum of ~12% at threshold and normally less than 5%, so the inaccuracy in this correction should typically be only a few percent. The $3S$ decay and any cascade contribution originating in an S state are, of course, unpolarized. Because of small signal sizes, the precision of the $3S$, $3P$, and $3D$ cross sections is typically ±10% at 1 standard deviation.

While many investigations of electron-impact excitation of atomic hydrogen have been carried out, most of these have been concerned with excitation of the $n = 2$ state. Only a few calculations and two experiments have been reported for $n = 3$ excitation. In addition to the Born[1] and Born-Ockhur approximations,[2] the theories include eikonel,[3] Glauber,[4,5] distorted-wave polarized orbital,[6] and impact-parameter[7] calculations, and modified Born approximations.[8,9] There have been no close-coupling calculations of $n = 3$ excitation except for those of Burke *et al.*[10] in which the $n = 3$ states were included in order to improve the accuracy of the cross sections for excitation of the $2p$ and $2s$ states. Both previous experiments[11,12] measured the relative excitation function for Hα for essentially the same energy range as the present work. In addition, an absolute measurement of the Hα cross section was made in Ref. 12 although the reported uncertainty of ±30% is probably less accurate than the Born theory at 500 eV. While part of the present work repeats those measurements, we have paid particular attention to the possible role of space charge and other sources of weak electric fields which can seriously distort the results. However, the real focus here is on obtaining the separate S, P, and D cross sections. The method used is described in Sec. II, the apparatus and procedures in Sec. III, and the results in Sec. IV. More detailed discussions of the work reported here can be found in Ref. 13.

II. TECHNIQUE OF TIME-RESOLVED CROSS-SECTION-RATIO MEASUREMENTS

The method employed to discriminate between the $3S$, $3P$, and $3D$ excitations is based on the different average delays between excitation and radiative decay. These states decay exponentially with lifetimes of approximately 158, 5.4, and 15.6 nsec, respectively. Owing to the large ratios of these lifetime values and to the difficulty of inferring the $3P$ excitation fraction for excitation

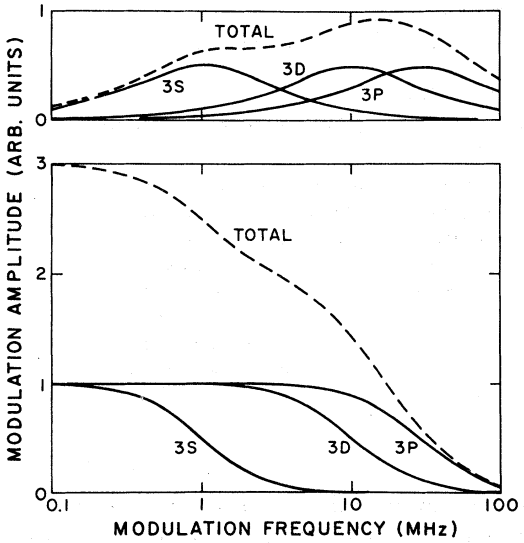

FIG. 1. Theoretical amplitude of modulated Balmer-α signals in the absence of cascade, as given by Eq. (1), for equal $Q_L B_L P_L$. The electron-beam intensity is assumed amplitude modulated at frequency f. The amplitudes of the in-phase signals are in the lower figure and out-of-phase amplitudes in the upper. These modulated radiation amplitudes are on the same intensity scale, but both are proportional to H density, optical efficiency, and other common factors.

pulse widths of a few nsec or longer, it would be very inefficient to use pulsed excitation and time-delay discrimination in the experiment. The modulated excitation technique, which has been used frequently to measure excited-state lifetimes,[14,15] yields very simple, direct relations between cross sections and the observed radiation. In addition it is much less sensitive to uncertainties in electron-beam time dependence and yields much greater average photon signals than the pulsed excitation method.

In the modulated excitation approach the electron beam is ~100% amplitude modulated (current $\propto\cos\omega t$) and the modulated fluorescence is detected. The time response of the fluorescence from each directly excited state is described by the same differential equation as is a low-pass RC filter. The modulated Hα fluorescence is described, in the absence of cascades, by[13,15]

$$I \propto \sum_{L=0,1,2} Q_{3L} B_{3L} P_{3L} \left(\frac{\cos(\omega\tau)}{1+(\omega\tau_{3L})^2} + \frac{\omega\tau_{3L}\sin(\omega\tau)}{1+(\omega\tau_{3L})^2} \right). \tag{1}$$

Here Q_{3L}, B_{3L} and τ_{3L} are the excitation cross section, branching ratio into Balmer α, and lifetime of each $3L$ state; and P_{3L} is the fraction $3/(3-P)$ of the total polarized fluorescence of state $3L$ that is detected at 90° to the electron beam. In the experiment we measure the in-phase ($\cos\omega\tau$) and 90° phase-shifted ($\sin\omega\tau$) fluorescence signals versus ω. The expected appearance of these signals, given by Eq. (1), is shown in Fig. 1 for the case of equal $Q_i B_i P_i$. It is clear from this figure that the different components are clearly separable on the basis of their distinctly different lifetimes or ω dependences. In the absence of cascades, either the in-phase or out-of-phase ω dependences could be used to obtain the cross-section ratios, so some consistency checks are possible. Note also that the desired $Q_i B_i P_i$ ratios are linearly related to the measured total signal, so the deconvolution procedure is quite straightforward. There are, as always, a variety of factors that complicate this simple model. These include cascading, H-beam motion out of the observed region, the apparatus time response, nonsinusoidal electron-beam amplitude modulation, Stark mixing by surface and space-charge electric fields, and the effect of coherences induced by the modulated excitation process. Fortunately, all of these effects are minor, and with the exception of cascade uncertainties accurate corrections can be made. We now consider these issues individually in more detail.

A. Cascading

Levels i with $n>3$ will populate the $n=3$ levels by cascade, mostly in single steps and to a minor extent compared to the direct excitation. Radiation from the cascade-fed segments of the $n=3$ populations is characterized by an expression containing the lifetimes of both the $3L$ and the ith states. For pulsed excitation we have the double-exponential expression

$$I_{\text{casc}} \propto Q_i B_{i\to 3L} \frac{\tau_{3L}}{\tau_i - \tau_{3L}} \left(e^{-t/\tau_i} - e^{-t/\tau_{3L}} \right), \tag{2}$$

where $B_{i\to 3L}$ is the branching ratio into state $3L$. For modulated excitation each exponential term yields a $\cos\omega t$ and $\sin\omega t$ term as in Eq. (1). The resulting total Balmer-α modulated intensity is then given by

$$I_{\text{total}} \propto \sum_{i,L} B_{3L} \left[\frac{Q_{3L} P_{3L}}{1+\omega^2\tau_{3L}^2} + \frac{Q_i B_{i\to 3L}\tau_{3L}}{\tau_i - \tau_{3L}} \left(\frac{1}{1+\omega^2\tau_{3L}^2} - \frac{1}{1+\omega^2\tau_i^2} \right) \right] \cos\omega t$$
$$+ B_{3L} \left[\frac{Q_{3L}\omega\tau_{3L}}{1+\omega^2\tau_{3L}^2} + \frac{Q_i B_{i\to 3L}\tau_{3L}}{\tau_i - \tau_{3L}} \left(\frac{\omega\tau_{3L}}{1+\omega^2\tau_{3L}^2} - \frac{\omega\tau_i}{1+\omega^2\tau_i^2} \right) \right] \sin\omega t\,. \tag{3}$$

The lifetimes and branching ratios are all accurately known, so the cascade correction terms in Eq. (3) have been calculated from assumed Q_i. (We neglect the uncertain but minor polarization correction to the already minor cascade signals.) Details are given in the Sec. IV.

B. H beam motion

The H beam has a thermal velocity distribution corresponding to the ~2500°K tungsten dissociation oven. This yields a mean thermal velocity of $\sim 1.5\times10^6$ cm/sec. The Balmer-α detection optics observes an image of the interaction volume that extends ~0.16 cm downstream from the electron beam, so an effective cutoff of the fluorescence occurs at ~260 nsec, owing to beam motion. When the entire beam velocity distribution and velocity dependence of the excitation probability is considered, this cutoff has a negligible effect on the observed $3P$ and $3D$ decays, but changes the apparent $3S$ decay into a form which is quite nonexponential. This observed decay can, however, be approximated very nearly by Eq. (1), with the total amount of observed S-state light reduced by a fraction γ, and the apparent lifetime τ' of the radiation shorter than its natural value τ. Thus, for the $3S$ state under the above conditions, the fraction γ of radiation lost is ~17%, and the apparent lifetime $\tau' = 135$ nsec, as compared with its natural value of $\tau = 158$ nsec. This detection cutoff also affects some of the cascade contributions, primarily the contributions involving the relatively long-lived $4S$ and $5S$ states. Since these cascade terms in Eq. (3) contribute only a few percent, they can also be adequately corrected by the above procedure.

C. Apparatus time response

When using pulsed or modulated timing techniques to measure lifetimes or cross sections, it is essential to determine the effective apparatus response $f(t-t')$ to an instantaneous input at t'. In essence, the apparatus generates time delay and spreading and this must be distinguished from that due to the excited-state lifetimes under study. In optical excitation experiments this apparatus response function has been measured by scattering the pumping beam from a suspension of particulates,[14] which are presumed to scatter instantaneously compared to the nanosecond time domain associated with atomic lifetimes. In electron excitation experiments short-lived atomic states has been utilized to provide test light with almost the same timing as the electron beam.[15] This requires very careful investigations, because of complexities such as cascading and electron time-of-flight spreading. We have utilized a metallic silver target to provide test light that should almost instantaneously follow electron impact. This target is well known to yield visible "transition radiation" for 30–100-keV electron-impact energies, and we observe copious amounts of blue radiation in our 15–500-eV range.[16] Based on simple transition-radiation theories, we expect this radiation to be emitted within less than a picosecond of electron impact.[16] Our primary concern is that a gradual contamination of the target surface might yield a slower fluorescence decay component. Several tests indicated that the observed radiation was predominately transition radiation, but we could not completely rule out the slow decay.[16] The consequence of such a slow-decay component of the test signal would be some intermingling of the measured $\sin\omega t$ and $\cos\omega t$ amplitudes in Eq. (3). Using this method of converting modulated electrons into modulated light we observed an instrumental response function roughly equivalent to a fixed apparatus time delay Δ plus a rolloff equivalent to a 5-nsec RC filter, i.e.,

$$f(t-t') \cong e^{-(t-t'-\Delta)/5\,\mathrm{nsec}} \quad \text{for } t \geq t'+\Delta$$
$$= 0 \quad \text{for } t < t'+\Delta\,. \tag{4}$$

This was close to the expected rolloff, due to photomultiplier and electronics response, so it further supported the assumption of negligible delay between electron impact and the test light.

The correction of the observed signals for the apparatus function is particularly simple in the modulation method. If the optical emission response to a pulse of electrons at t' is defined as $F(t-t')$, then the observed signal is

$$S(t) = \iint f(t-t'')F(t''-t')I(t')\,dt''\,dt'\,,$$

where $I(t')$ is the time-dependent electron current. The measured Fourier amplitude S_ω of $S(t)$ is then given, for $I(t') = \cos\omega t'$, by $f_\omega F_\omega$, the product of the Fourier amplitudes of $f(t-t')$ and $F(t''-t')$. The measurements using metallic silver establish f_ω, since in this case $F(t''-t') = \delta(t''-t')$, so we simply divide S_ω by f_ω to obtain the desired F_ω due to Balmer-α excitation. (The time delay Δ causes no difficulty, and for convenience can be adjusted to ~0 by compensating with a length of cable.) The Balmer-α light detected in phase with the observed signal from silver corresponds to the amplitude of the $\cos\omega t$ term in Eq. (3), and that with a 90° phase delay to the $\sin\omega t$ term. It is important to note that the accuracy of ~1° at 30 MHz obtained in this procedure corresponds to about 0.1-nsec time uncertainty. It is also important to have a rapid apparatus response compared to the

shortest measured lifetime to provide a clear separation of the rapid decay terms in Eq. (3).

D. Modulation distortions

It is quite unlikely that the electron-beam current in the interaction volume is given by $A + B \times \cos\omega t$, without higher harmonics, even if the modulation voltages applied to the electron gun are free from harmonics. The higher harmonics are phase shifted and attenuated according to Eq. (3), with $n\omega$ in place of ω, where $n = 2, 3, \ldots$, so it is important to avoid measuring the resultant signals. This is easily done by electronic filtering in the lock-in detection apparatus. The amplitude of the fundamental will also depend on gun voltages and electron time of flight across the interaction volume. Here the metallic-silver signals are again essential, as they provide a calibration of the modulation amplitude of the fundamental at all operating conditions. In essence the Balmer-α modulation amplitudes ($F_\omega f_\omega$) are measured relative to those from the silver (f_ω) at every frequency and gun energy.

E. Stark mixing

Because of the small energy separations of the $n = 3$ levels, an electric field in the interaction region as small as 1 V/cm could mix the populations of these levels in such a way that the Q_{3L} coefficients obtained from the phase-shift technique will not reflect the true individual excitation cross sections. The average Balmer-α intensity for dc or modulated excitation will also be affected, since altered populations of the $3P$ versus $3S$ and $3D$ states will change the branching into Balmer α versus Lyman β. The major expected source of electric field in our interaction region is the space-charge field produced by the negatively charged electron beam. Accordingly, at every energy and frequency, the modulation and dc data are extrapolated to zero electron current. Other possible stray fields in the interaction region due to surface potentials and field penetration have been examined by placing a known electric field strength in three orthogonal directions in the interaction region, and looking for the symmetry of the Hα signal versus the sign of the field strength. (The average electron-impact energy in the interaction volume is kept constant.) Calculations of Stark mixing, including coherent excitation of different $3L$ states, predict symmetric quadratically rising Hα signals for fields transverse to the electron beam (owing to net transfer of $3P$ population into $3S$ and $3D$), and somewhat asymmetric signals for fields parallel to the electron beam (owing to coherent excitation[13,17]). At about ± 2 V/cm and ≥ 200-eV impact energies, corresponding to our test measurements, the asymmetry is minor and included in the analysis. Thus the observed Hα signals should rise essentially symmetrically as positive and negative fields are applied in each orthogonal direction. Residual fields due to surface potentials or field penetration can thus be detected as a shift of the signal minimum to nonzero applied field. No such shifts were found, so the effects of the possible mixing on modulation amplitudes as well as total signals will not be discussed further here. The expected changes in total Hα intensity are calculated in Refs. 13 and 17 and the measurements are reported in Ref. 13.

F. Modulated coherent excitation

The theory of coherent excitation by modulated light or electrons is well developed, and a number of experiments have used these techniques to investigate excited-state lifetimes and structure.[18-20] These resonances are only observed if net polarization or alignment population differences result from the excitation, since the resonances are discernible as changes in fluorescence anisotropy. In discussing Eqs. (1) and (3) we have ignored such coherences since we do not expect very large polarizations to be induced by the electron-impact excitation and these effects should be unimportant at the present experimental uncertainties.

III. EXPERIMENTAL DETAILS

In this crossed-beam experiment, a beam of atoms is excited by an orthogonal beam of electrons, and the resultant Hα intensity is measured at right angles to both beams. The measurements are carried out in the hydrogen-beam apparatus described by Long *et al.*,[21] who used it to measure excitation to the $2P$ state by observing Lyman-α radiation emitted at 90° to the plane of two beams. The primary modification to the apparatus for the present work was the substitution of Balmer-α detection optics in place of the Lyman-α detector. Other details which differ from those treated in Ref. 21 are discribed below.

A. Backgrounds

The H beam was chopped by quartz blades for the relative Balmer-α excitation-function measurements, so steady background sources did not influence the results (see Refs. 13 and 21 for details). For the modulated-excitation measurements, the steady-state backgrounds were eliminated from the signal without chopping the H beam.

The H density in the interaction volume is $\sim 10^8/\text{cm}^3$, while the background gas density, ac-

cording to ionization gauges, is typically $\sim 3\times10^{8}/cm^{3}$, with half of this due to the H-beam gas load. In the relative excitation-function measurements, when the H beam was chopped and the H-beam signal and the background gas signal were independently determined, the latter was found to be typically 1–3% of the H-beam signal. This should be primarily due to dissociative excitation of H_2. Both this and the H_2 component of the beam signal (typically ~1%) require corrections in the relative excitation-function measurement, following procedures described in Ref. 21. In the modulated-excitation measurements the count rate and S/N is too small to allow H-beam chopping as well. Thus some 2–4% of the reported modulated signals are due to dissociative excitation of H_2 to produce Balmer α (for energies above the 17 eV threshold for this process). At the typical ±10% accuracy level of the present modulation-signal results, this is not a significant correction.

B. Optics

The optical system consists of a pair of 50-mm focal length, $f/1.2$ camera lenses focused at infinity, with the interaction chamber in the focal plane of one lens and a slit mechanism in the focal plane of the other. (The H beam is 5×5 mm cross section and the electron beam ~2 mm in diameter in the interaction volume.) The shape of the electron beam was tested by moving the slits; it was ascertained that all of the electrons traversed the H beam within the observed volume for all collision energies. A 6563-Å interference filter of ~15-Å half-width was used to isolate the Hα line, and a quartz light pipe was used behind the slits to scramble the image and provide a uniform detector sensitivity versus interaction-chamber position. The light pipe also provides transmission across the thermal gradient to the cooled in Ga-As photomultiplier. The photomultiplier pulses are amplified with ~1-nsec rise time, 50-Ω amplifiers and counted with fast discriminators.

A major problem in these Hα measurements arises from the use of a tungsten furnace operated at ~2500°K to dissociate the hydrogen at the beam source. The power consumption of approximately 600 W is converted into a great amount of visible radiation, which must be carefully shielded from the detection optics. In practice the signals of typically 50 counts/sec exceed this background source by about a factor of 3 when the interaction chamber is coated with aquadag and carefully shielded by a series of baffles.

C. Electronics

The relative excitation-function measurements utilize photoelectron counting, with the counts accumulated alternately in two counters as the H beam is chopped with ~50% duty cycle. Care was taken to ensure equal counting times for the two counters. Details for equivalent Lyman-α measurements are given in Ref. 21.

For the modulated-excitation measurements it is necessary to amplitude modulate the electrons at selected frequencies from 0.1–30 MHz and to detect the rf phase of the photomultiplier pulses with nanosecond or subnanosecond timing accuracy to separate the $\cos\omega t$ and $\sin\omega t$ amplitudes. Further, the noise level must be determined primarily by counting statistics at a count rate as low as several counts per second. The essentials of the method used are the following. A modulation voltage $\propto \cos\omega t$ is applied to the electron-gun grid, providing typically 80% amplitude modulation at the fundamental frequency. The photomultiplier discriminator output, consisting of pulses distributed in time as $A + B\cos(\omega t+\phi)$, is used to open a gate (balanced modulator) for about 3 nsec [A, B, and ϕ are related to the constants in Eq. (3)]. The gate transmits the instantaneous value of a voltage $\propto \cos(\omega+f)t$, where $f = 1$ kHz. This voltage is generated by a single sideband generator, and is carefully maintained free from rf harmonics. In essence the gate multiplies the sideband-generator output by the experimental signal, producing a resultant signal containing a low-frequency component $B\cos(ft+\phi)$ with the experimental rf phase angle ϕ transferred to the 1-kHz modulation and corresponding to a much longer time interval. The primary reason for utilizing this single-sideband method of frequency heterodyning is that low, fixed-frequency lock-in detection in the convenient 1-kHz region could be used for all ω values. Thus the pulses out of the gate are amplified, low-pass filtered, and fed into two lock-in detectors operating at 1 kHz. The reference phase of one lock-in was adjusted to yield a null for the silver-target signal; it thus detected the $\sin\omega t$, or "out-of-phase" modulation amplitude of Eqs. (1) and (3). The other lock-in reference was shifted 90° to measure the $\cos\omega t$ "in-phase" modulation amplitude.

Since the photomultiplier signal rates are typically 50 counts/sec, it is essential to use a linear averaging technique such as lock-in detection. In addition, there is a great deal of noise inherent in the wide bandwidth amplification of the ~3-nsec pulse out of the gate. In order to obtain a statistical noise level, unaffected by amplifier noise, a second gate is used to transmit the amplified and somewhat spread pulse from the first gate. Thus the noise from the first amplifier stage is only transmitted to the lock-in's when a photomultiplier count occurs. With this arrangement the amplifier

TABLE I. Data reduction.

Electron energy (eV)	Relative [a] Hα(90°) (eV)	From modulation-amplitude measurements $I_{3S}(90°)$ [b] Hα(90°)	$I_{3P}(90°)$ Hα(90°)	$I_{3D}(90°)$ Hα(90°)	$I_{CASC}(90°)$ Hα(90°)	Polarization corrections $\frac{\langle I_{3P}\rangle}{I_{3P}(90°)}$	$\frac{\langle I_{3D}\rangle}{I_{3D}(90°)}$	Normalized cross sections Q_{3S} $(10^{-2}\pi a_0^2)$	0.118 Q_{3P} $(10^{-2}\pi a_0^2)$	Q_{3D} $(10^{-2}\pi a_0^2)$	Direct Hα $(10^{-2}\pi a_0^2)$	Hα cascade $(10^{-2}\pi a_0^2)$
10	3 ± 5	...	...	...	...	...	...					
13.8	330 ± 9	0.305 ± 0.03 0.31 ± 0.04	0.072 ± 0.04 0.070 ± 0.04	0.580 ± 0.05 0.576 ± 0.06	0.044	0.88	0.86	2.2 ± 0.2 1.2 ± 0.2	0.45 ± 0.2 0.44 ± 0.2	3.5 ± 0.3 3.5 ± 0.3	6.15 ± 0.35	0.31
18.8	343 ± 6	0.327 ± 0.03 0.291 ± 0.03	0.118 ± 0.03 0.135 ± 0.04	0.506 ± 0.05 0.525 ± 0.06	0.050	0.91	0.89	2.4 ± 0.2 2.15 ± 0.2	0.79 ± 0.2 0.90 ± 0.2	3.3 ± 0.3 3.4 ± 0.3	6.5 ± 0.30	0.37
29	300 ± 5	0.223 ± 0.03 0.190 ± 0.03	0.152 ± 0.03 0.208 ± 0.04	0.561 ± 0.05 0.538 ± 0.06	0.065	0.94	0.93	1.45 ± 0.2 1.23 ± 0.2	0.92 ± 0.2 1.26 ± 0.2	3.4 ± 0.3 3.2 ± 0.3	5.7 ± 0.23	0.42
39	259										5.2 ± 0.20	0.37
49	244 ± 7	0.243 ± 0.025 0.237 ± 0.03	0.269 ± 0.03 0.268 ± 0.04	0.423 ± 0.04 0.430 ± 0.06	0.065	0.96	0.98	1.28 ± 0.15 1.25 ± 0.15	1.36 ± 0.15 1.35 ± 0.15	2.2 ± 0.25 2.2 ± 0.25	4.8 ± 0.20	0.34
80	171 ± 5	0.221 ± 0.02 0.252 ± 0.025	0.245 ± 0.02 0.276 ± 0.03	0.457 ± 0.03 0.397 ± 0.04	0.076	0.99	1.00	0.81 ± 0.10 0.93 ± 0.10	0.89 ± 0.10 1.00 ± 0.10	1.68 ± 0.15 1.47 ± 0.15	3.38 ± 0.15	0.28
120	126 ± 4										2.50 ± 0.12	0.20
202	92 ± 3	0.313 ± 0.02 0.276 ± 0.02	0.385 ± 0.025 0.400 ± 0.025	0.216 ± 0.03 0.238 ± 0.04	0.087	1.01	1.05	0.62 ± 0.05 0.55 ± 0.05	0.77 ± 0.05 0.80 ± 0.05	0.45 ± 0.07 0.49 ± 0.07	1.84 ± 0.10	0.17
303	68 ± 3										1.33 ± 0.09	0.14
506	45 ± 2	0.232 ± 0.025 0.225 ± 0.035	0.164 ± 0.04 0.209 ± 0.06	0.164 ± 0.04 0.209 ± 0.06	0.093	1.03	1.08	0.225 ± 0.2 0.215 ± 0.2	0.51 ± 0.15 0.47 ± 0.15	0.17 ± 0.05 0.22 ± 0.05	0.90	0.09

[a] This is an average of four data sets, normalized to each other at 38 eV. The uncertainty is 1 standard deviation of the mean.
[b] $I_{3L}(90°)$, the observed Hα signal, is identified as $Q_{3L}B_{3L}P_{3L}$; the × + □ and × fits, as in Figs. 2 and 3, are given consecutively.
[c] From Born-approximation calculations. The cascade contributions are treated as unpolarized.

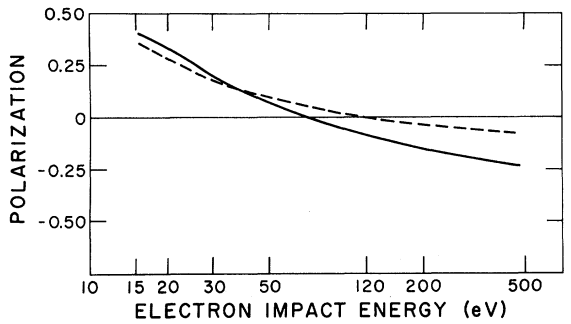

FIG. 2. Assumed polarization of $3D$ (dashed line) and $3P$ (solid line) contributions to Hα, calculated by Born approximation without cascading .

noise is below the statistical noise even at count values as low as 1/sec. It is noteworthy that the time-measurement accuracy is considerably better than 1 nsec with this very low noise level. Additional minor complications and apparatus and analysis details are discussed in Ref. 13.

IV. DATA REDUCTION AND ANALYSIS

Both the continuous- and modulated-excitation measurements were made for a number of electron currents (I) in each energy range. Since the Stark mixing is proportional to the square of the electric field, except for minor linear terms due to coherent excitation, the observed signal variations due to space-charge fields should extrapolate to field-free conditions in proportion to I^2. The observed variations were consistent with this expected behavior. The observed signal variations, for typical currents of 10–40 μA, are normally 15% or less, with typical extrapolations of ~5% required. All of the data subsequently presented have been extrapolated to $I = 0$. The observed I dependences can be found in Ref. 13. The measured total Hα relative excitation function Hα(90°), corrected for 1–2% contributions from H_2 in the beam, is given in column 2 of Table I.

The data reduction and analysis are complicated by the fact that the two types of experimental measurements, direct current and modulated excitation, must be reduced and analyzed with self-consistent cascade and polarization corrections. Since the accuracy of the data is insufficient to determine independently any of the cascade contributions [Q_i in Eq. (3)], we have used estimated cascading fractions to establish the three cross sections Q_{3L}. The cross-section ratios Q_{nL}/Q_{3L} for $n > 3$ were fixed by using the Born approximation, since little else is available and it appears probably that the Born *ratios* may be reasonably accurate. The following cross-section ratios were taken from Vainshtein[1]; $4S/3S$, 0.36; $5S/3S$, 0.17; $4P/3P$, 0.36; $5P/3P$, 0.17; $6P/3P$, 0.095; $4D/3D$, 0.47; $5D/3D$, 0.27. Neither the $4F$ nor $5F$ excitation cross sections have been calculated by Vainshtein, but they are expected to be negligible.[13] Cascading from higher states is deemed insignificant.

The Q_i in Eq. (3) can be expressed in terms of the Q_{3L} using these assumed cross-section ratios and time-of-flight corrections of Sec. II B. The $B_{i\to 3L}$ are well known and Born-theory polarizations from Ref. 10, which are shown in Fig. 2, have been used to calculate $P_{3L} = 3/(3-P)$. Thus Eq. (3) can be expressed in terms of the three unknowns Q_{3S}, Q_{3P}, Q_{3D}, or two cross-section ratios and a signal-magnitude factor. These unknown ratios can then be determined by a least-squares fitting of Eq. (3) to the modulation data. However, the sensitivity of the resultant ratios to the assumed cascading is better demonstrated by the following iterative procedure, which we apply to the 500-eV data as an example. In Fig. 3, the modulation-amplitude data for 500-eV electron energy are compared to a least-squares fit using Eq. (1), or Eq. (3) without cascade terms. The inferred ratios of $Q_{3L}B_{3L}P_{3L}$ are given in the caption. Using these (incorrect) ratios and the above Born ratios of Q_{NL}/Q_{3L}, the cascade contributions shown in Fig. 4 are obtained using Eq. (3) and the minor time-of-flight correction described in Sec. II B (the cascading is assumed unpolarized). The cor-

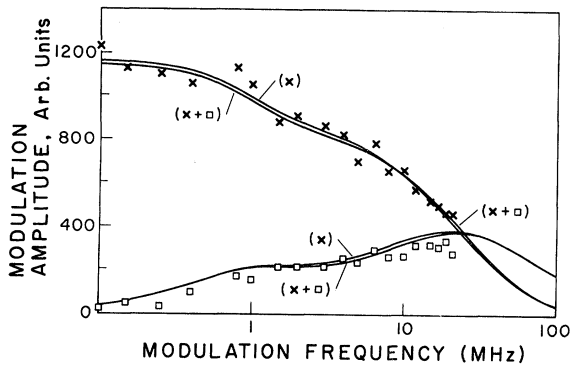

FIG. 3. Measured in-phase or cosωt modulation amplitudes (×) and out-of-phase amplitudes (□) versus modulation frequency for electron-impact energy of 500 eV. These amplitudes are relative to signals from a metallic silver target, and so are due to the Hα decay rate only. The solid lines labeled × and × + □ are the theoretical least-squares fits using Eq. (1) corrected for H-beam motion; the × from fitting only the in-phase data and the × + □ from fitting in- and out-of-phase data. The fitting coefficients $Q_{3L}B_{3L}P_{3L}$ in order $3S$, $3P$, and $3D$ are 337 ± 29, 580 ± 35, 234 ± 56 for the × + □ line and 331 ± 40, 543 ± 46, and 292 ± 65 for the × line. (The units are relative.) These uncertainties are 1 standard deviation from the least-squares fitting program.

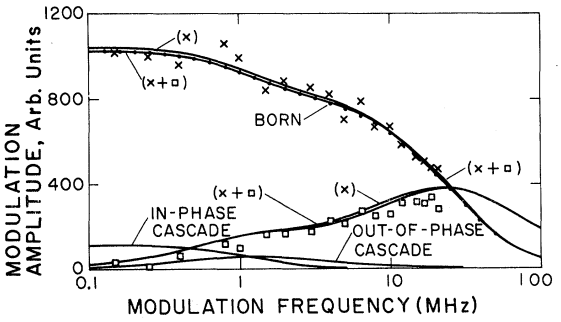

FIG. 4. Same as Fig. 2, except that Eq. (3) is used and the cascading indicated at the bottom of the figure has been included in the theoretical fit. The $Q_{3L}B_{3L}P_{3L}$ coefficients obtained from the least-squares fitting are 275±28, 603±34, and 194±45 for the ×+□ case and 269±40, 567±45, and 251±66 for the × line. The relative units are the same as in Fig. 3. The points labeled Born correspond to Born-approximation ratios of $Q_{3L}B_{3L}P_{3L}$ (281, 579, and 212, respectively) and the same total Hα signal.

rected ratios of $Q_{3L}B_{3L}P_{3L}$ products are then obtained from a least-squares fit of Eq. (1) to these cascade-corrected data, with the results shown in Fig. 4. This iterative procedure converges well within the data accuracy in one step. From this example it can be seen that the cascading corrections typically decrease Q_{3P} by only a few percent but decrease Q_{3S} and Q_{3D} by about 20%. This is because the lifetimes of the cascading states are 17 nsec or longer, so that the high-frequency data almost uniquely fix the cross section of the 5.4-nsec-lifetime $3P$ state. The total cascade contribution to the observed Hα intensity is seen at the left edge of Fig. 4, since 0.1 MHz is effectively the zero frequency or steady-state limit.

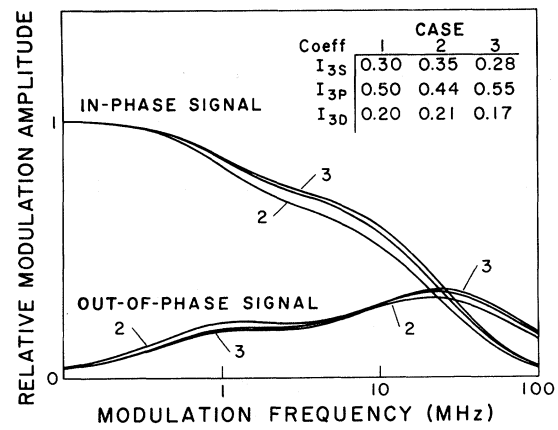

FIG. 5. Calculated modulation amplitudes for several ratios of $Q_{3L}B_{3L}P_{3L}$ in the neighborhood of those in Figs. 3 and 4. The ratios used are indicated in the inset as $I_{3L} = Q_{3L}B_{3L}P_{3L}/\sum_L Q_{3L}B_{3L}P_{3L}$.

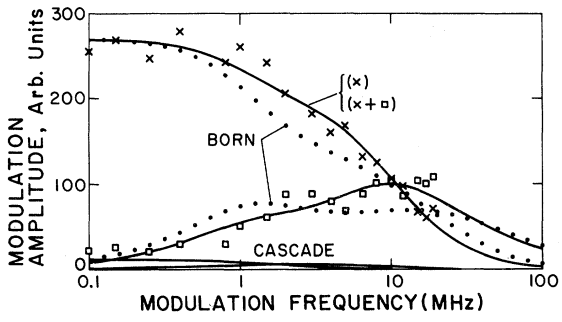

FIG. 6. Same as Fig. 4, except for an electron-impact energy of 15 eV. The $Q_{3L}B_{3L}P_{3L}$ values are 90±8, 21±11, and 172±14 for the ×+□ fit, 92±12, 21±14, and 171±20 for the × fit, and 158, 72, and 65 for the points obtained using the Born approximation.

The least-squares fitting procedure yields the statistical uncertainties in $Q_{3L}B_{3L}P_{3L}$ given in the captions of Figs. 3 and 4. These 1σ uncertainties in the portion of the total Hα attributed to each state are between 5–20%, which is typical for one such data set. That they do not appreciably improve from Fig. 3 to 4 when the cascade correction is included, indicates that the data are much too noisy to yield any independent cascade infor-

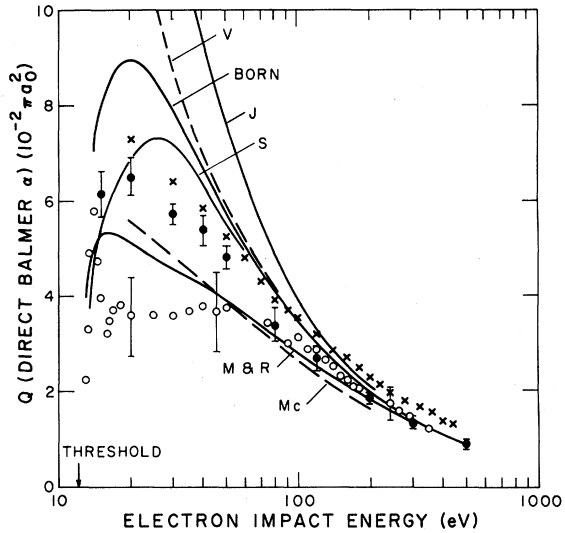

FIG. 7. Total normalized Hα excitation cross section. The theories, the present results (●), and the experimental results of Kleinpoppen and Kraiss, Ref. 11 (○), are for direct $n=3$ excitation. The results of Walker and St. John, Ref. 12 (×), include a small cascade component are are also not corrected for polarization. The theoretical results are as follows: Born approximation, Vainshtein, Ref. 1 (Born); distorted wave, Vainshtein, Ref. 22 (V); Morrison and Rudge, Ref. 8 (M and R); distorted-wave polarized orbital, McDowell *et al.*, Ref. 6 (Mc); Jamieson, Ref. 7 (J); unitarized Born, Somerville, Ref. 9 (S).

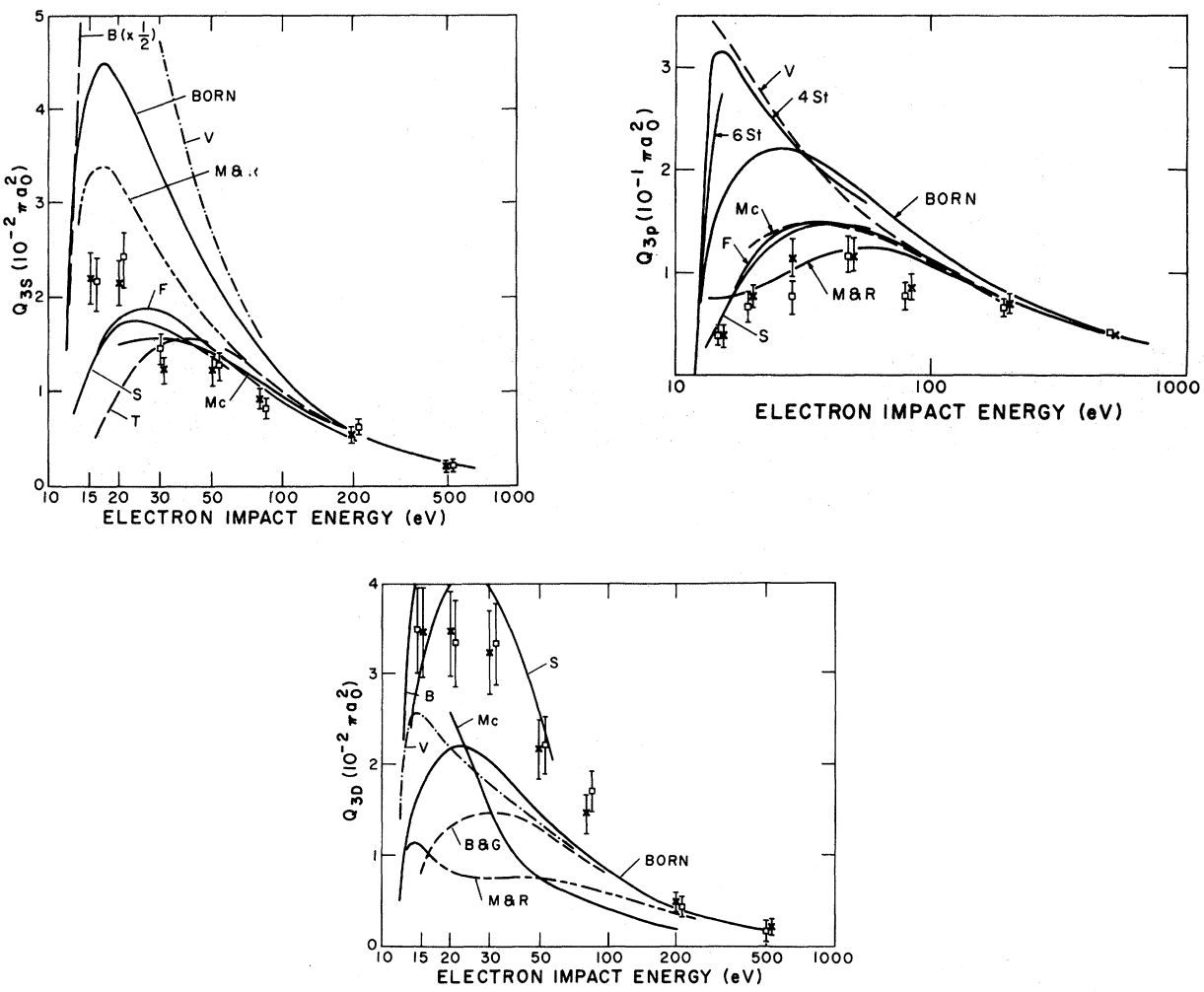

FIG. 8. $3S$-, $3P$-, and $3D$-state direct excitation cross sections from the present measurements are given as × and □ using the in-phase and in-phase-plus–out-of-phase fits as in Figs. 3 and 5; the □ should be more accurate but the difference is an indication of the data reliability. The theoretical lines are coded as in Fig. 7, with the additions of the close-coupling results of Burke *et al.*, Ref. 10 (B) or (4-St) or (6-St): Eikonel, Flannery, and McCann, Ref. 8 (F): Glauber approximation, Bhadra and Ghosh, Ref. 5 (B and G); Glauber approximation, Tai *et al.*, Ref. 4 (T). The $3P$ cross section reported in Fig. 6 of Ref. 4 has not been included as it is clearly misplotted. The Ochkur-approximation results of Gumble, Ref. 2, have not been included as they are close to the Born values.

mation. In Fig. 5 the sensitivity of the modulation amplitudes to changes in the cross-section ratios is shown, for ratios of $Q_{3L}B_{3L}P_{3L}$ values in the neighborhood of those in Figs. 3 and 4. The changes in Fig. 5 which result from the 15% ratio variations indicated are comparable to the scatter in the data of Fig. 4, indicating that the statistical uncertainties of 5–20% are reasonable uncertainty estimates.

As an additional example of the raw data and a set of quite different cross-section ratios, the modulation amplitudes for 15-eV collision energy are shown in Fig. 6. Note that the differences between the data and the modulation amplitudes predicted by the Born approximation are now quite large.

The ratios $I_{3L}(90°)/H\alpha(90°)$ and $I_{\text{casc}}(90°)/H\alpha(90°)$ for all of the data are given in columns 3–6 of Table I. These ratios for 90° detection can be corrected to isotropically averaged intensity ratios using the assumed Born-approximation polarizations of the $3P$ and $3D$ contributions, plus the assumption of unpolarized cascade contributions (the $3S$ decay is unpolarized). The Born-approximation polarizations calculated in Ref. 10 are given in Fig. 2, and the polarization corrections in columns

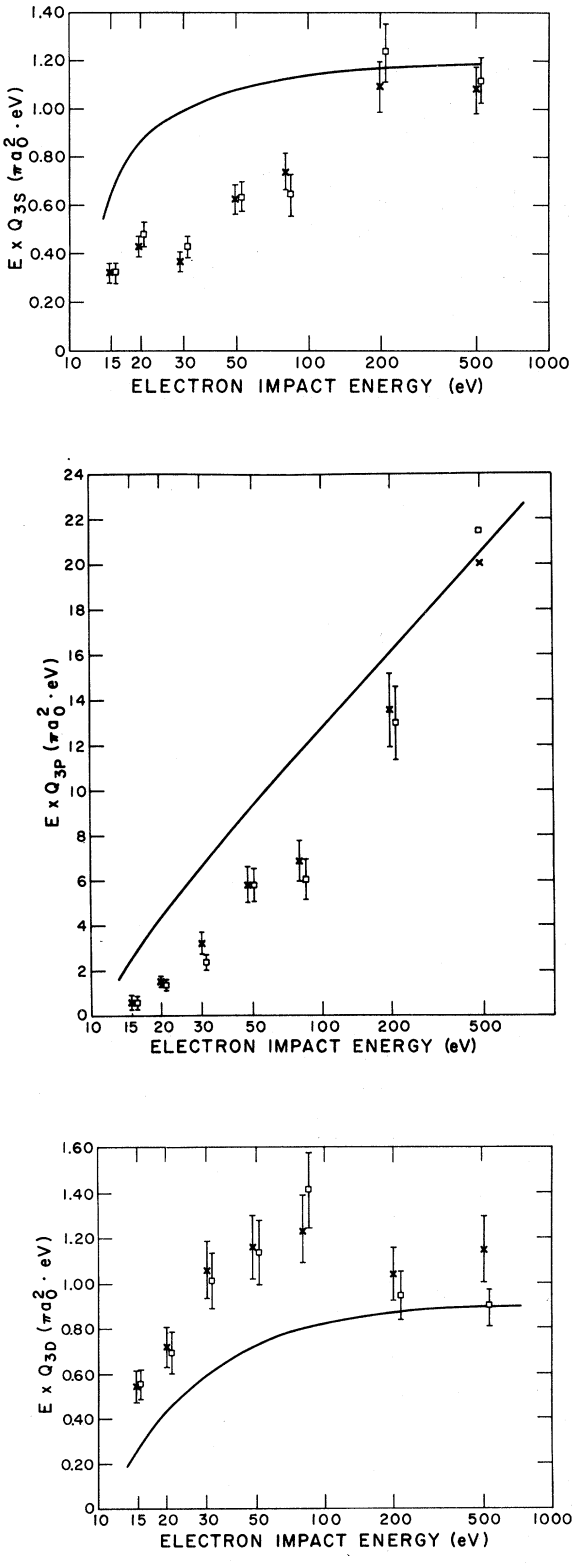

FIG. 9. Cross section times energy, QE, for the direct $3S$, $3P$, and $3D$ excitations. The expected high-energy behavior is given by the Born QE lines.

7 and 8 of Table I. Multiplying column 2 by column 3 (or 6) of Table I then yields the relative excitation cross section for the $3S$ state (or cascading). Multiplying columns 2, 4, and 7 yields $B_{3P}(0.118)$ times the $3P$ excitation cross section in the same relative units. Similarly, the product of columns 2, 5, and 8 yields the relative $3D$ excitation cross section. The sum $Q_{3S} + B_{3P} Q_{3P} + Q_{3D}$ in these relative units has been normalized to the same weighted sum of Born cross sections at 500 eV, by multiplying the relative units by 2.15×10^{-4}. The resulting Q_{3L} are given in columns 9–11, the $\sum Q_{3L} B_{3L}$ in column 12, and the cascade contributions to Hα in column 13 of Table I. The direct Hα cross section in column 12 is compared to theories and other measurements in Fig. 7.[22] The individual Q_{3S}, Q_{3P}, and Q_{3D} are compared to available theories in Fig. 8. The high-energy results and uncertainty in normalization are more readily seen in plots of QE versus E, which are given in Fig. 9.

V. CONCLUSIONS

The Hα excitation cross sections from three experiments are compared in Fig. 7. The present results and those of the Kleinpoppen and Kraiss[11] are corrected for polarization and cascading, which lowers the cross section in the low versus high-energy region by about 10%. If Walker and St. John's results[12] are normalized to the Born theory at high energy, as are the other measurements, they are about 15% below the present results in the low-energy region. Although cascading and polarization corrections would make this discrepancy somewhat greater, this is within the combined experimental uncertainties. This minor difference as well as the quite different energy dependence reported by Kleinpoppen and Kraiss[11] could be due to electric field mixing of the $3L$ states in the other experiments. With increasing collision energies the $3P$ cross section becomes larger relative to $3S$ and $3D$, causing an increase in the magnitude of the electric field dependence of the Hα signal. Combined with surface or space-charge fields, this could cause a larger relative increase in Hα at high energy. Of course, the magnitudes of any residual fields could also vary with electron-beam energy, causing variations in the mixing.

The high-energy behavior of the reported $3S$, $3P$, and $3D$ excitation cross sections is compared to the Born approximation in Fig. 9. The agreement of the measured Q_{3P}/Q_{3S} and Q_{3P}/Q_{3D} ratios with the Born theory is gratifying, even though the experimental uncertainty is rather large. That the dipole-allowed $3P$ cross section approaches the Born value from below is consistent with obser-

vations for $^1H(2P)$ and other dipole-allowed excitations.[23] Similarly, the fact that Q_{3S} falls below the Born cross section at lower energies is consistent with H(2S) excitation. In the low-energy region of $n = 3$ excitation thresholds, shown in Fig. 8, the 3S and 3P cross sections fall below the Born value by a factor of 2 to 3, which is again very similar to H(2S), H(2P), and many other excitation cross sections. The behavior of Q_{3D} is quite different in that it greatly exceeds the Born cross section at low energy. The general behavior is only obtained by one of the available theories. Somerville, using Seaton's unitarized Born, or Born-II, method obtains the general pattern of observed cross sections. This calculation includes coupling of all $n = 1$, 2, and 3 levels, and the author explains the large 3D cross section as being due primarily to $1S \rightarrow 2P \rightarrow 3D$ (in a single collision). A similar enhancement of n^1D cross sections in He may be attributed to a similar $1S \rightarrow 2P \rightarrow nD$ excitation process.[24] This intermediate-state coupling mechanism is discussed in detail in Ref. 25.

The relatively few theoretical calculations, with widely varying results, and our major disagreement with the only close-coupling calculations, indicate that these cross sections are not well understood. The close-coupling method, which has been so successful for $n = 2$ excitation, may in fact be inadequate for $n = 3$, owing to the small energy spacing to $n > 3$ levels. On the other hand, Somerville's results based on a very simple approximation are quite encouraging. It is hoped that the present results will stimulate investigations of these issues.

ACKNOWLEDGMENTS

We wish to thank D. Truhlar for valuable discussions of the theories. This work was supported by the National Science Foundation through grants GP 39308X and GP 17174 to the University of Colorado.

---

*Present address: Fakültat für Physik, Universitat Bielefeld, 4800 Bielefeld, West Germany.
†Staff member, Laboratory Astrophysics Division, National Bureau of Standards.

[1]L. A. Vainshtein, Opt. Spektrosk. 18, 947 [Opt. Spectrosc. (USSR) 18, 538 (1965)]. The modifications of B. L. Moiseiwitsch and S. J. Smith, Rev. Mod. Phys. 40, 238 (1968), have been used.
[2]R. A. Grumble, J. Phys. Soc. Jpn. 27, 973 (1968).
[3]M. R. Flannery and K. J. McCann, J. Phys. B 7, L522 (1974).
[4]H. Tai, R. H. Bassel, E. Gerjuoy, and V. Franco, Phys. Rev. A 1, 1819 (1970).
[5]K. Bhadra and A. S. Ghosh, Phys. Rev. Lett. 26, 737 (1971).
[6]M. McDowell, V. Myerscough, and U. Narian, J. Phys. B 7, L195 (1974); M. McDowell, R. Syms, L. Morgan, and V. Myerscough in *Tenth International Conference on the Physics of Electronic and Atomic Collisions: Invited Papers and Progress Reports, 1975.*
[7]M. J. Jamieson, Mol. Phys. 29, 633 (1975).
[8]D. J. T. Morrison and M. R. H. Rudge, Proc. Phys. Soc. Lond. 89, 45 (1966).
[9]W. B. Somerville, Proc. Phys. Soc. Lond. 82, 446 (1963).
[10]P. G. Burke, H. M. Schey, and K. Smith, Phys. Rev. 129, 1258 (1963), four-state calculation; P. G. Burke, S. Ormonde, and W. Whitaker, Proc. Phys. Soc. Lond. 92, 319 (1967), six-state calculation.
[11]H. Kleinpoppen and E. Kraiss, Phys. Rev. Lett. 20, 361 (1968).
[12]J. D. Walker, Jr. and R. M. St. John, J. Chem. Phys. 61, 2394 (1974).
[13]A. H. Mahan, Ph.D. thesis (University of Colorado, 1974) (unpublished).
[14]F. Duschinsky, Z. Phys. 81, 7 (1933); W. Demtroder, Z. Phys. 166, 42 (1962).
[15]G. M. Lawrence and B. D. Savage, Phys. Rev. 141, 67 (1966).
[16]A. H. Mahan and A. Gallagher, Rev. Sci. Instr. (to be published).
[17]R. A. Krotkov, Phys. Rev. A 12, 1793 (1975).
[18]G. Breit, Rev. Mod. Phys. 5, 91 (1933); P. A. Franken, Phys. Rev. 121, 508 (1961); B. Budick, *Advances in Atomic and Molecular Physics* (Academic, New York, 1967), Vol. 3, Chap. 3.
[19]A. Corney and G. W. Series, Proc. Phys. Soc. Lond. 83, 207 (1964); E. G. Aleksandrov. Opt. Spektrosk. 16, 377 [Opt. Spectrosc. (USSR) 16, 209 (1964)]; L. Armstrong, Jr. and S. Feneuille, J. Phys. B 8, 546 (1975).
[20]O. Nedelec, M. Deschizeaux, and J. Pebay-Peyroula, C. R. Acad. Sci. (Paris) 257, 3130 (1963).
[21]R. L. Long, D. M. Cox, and S. J. Smith, J. Res. Natl. Bur. Stand. (U.S.) A 72, 521 (1968).
[22]L. A. Vainshtein, Opt. Spektrosk. 11, 301 [Opt. Spectrosc. (USSR) 11, 163 (1961)].
[23]D. Leep and A. Gallagher, Phys. Rev. A 10, 1082 (1974).
[24]A. F. J. van Raan, J. P. de Jongh, J. van Eck, and H. G. M. Heideman, Physica 53, 45 (1971).
[25]D. G. Truhlar, Phys. Rev. A 4, 1886 (1971).